Applied Surface Science 473 (2019) 578–588

Contents lists available at ScienceDirect

Applied Surface Science

journal homepage: www.elsevier.com/locate/apsusc

Full Length Article

Au nanoparticles decorated on activated coke via a facile preparation for efficient catalytic reduction of nitrophenols and azo dyes

Yukui Fu[1], Piao Xu[1], Danlian Huang[1], Guangming Zeng*, Cui Lai*, Lei Qin, Bisheng Li, Jiangfan He, Huan Yi, Min Cheng, Chen Zhang

College of Environmental Science and Engineering, Hunan University, Changsha 410082, PR China
Key Laboratory of Environmental Biology and Pollution Control, Hunan University, Ministry of Education, Changsha 410082, PR China

ARTICLE INFO

Keywords:
Au nanoparticles
Activated coke
Catalytic reduction
Nitrophenols
Azo dyes

ABSTRACT

Activated coke (AC) exhibits excellent properties with a graphite-like layer crystallite structure and possesses mesopore and macropore structures, which can reduce the influence of internal diffusion on the general rate of adsorption and catalytic process greatly. In this work, AC was served as a support for gold nanoparticles (Au NPs) anchoring to prepare Au/AC catalysts via a facile synthesis using ascorbic acid as a mild reducing agent. The morphology and structure of catalysts were characterized by XRD, TEM, FTIR, and XPS analysis. Our experiment results showed that the abundant functional groups on the surface of AC play a vital role in the immobilization of Au NPs. Au/AC was employed as a highly efficient catalyst with a rate constant of 0.1916 s^{-1} for the reduction of 4-nitrophenols by $NaBH_4$. Au/AC was also tested for the catalytic reduction of other nitrophenols (2-nitrophenol and 2,4-dinitrophenol) and azo dyes (congo red, methyl orange and erichrome black T), demonstrating that Au/AC exhibited superior catalytic efficiency compared with other Au NPs catalysts. The catalysts showed good reusability, with conversion of 84% in the reduction of 4-NP in 20 s after six cycles. The Au/AC with high TOF has potential to be a workable and efficient catalyst in industrial applications. Present study not only provides a facile preparation route of catalysts using AC as a promising support, but also sheds light on the understanding of mechanism of the synergistic effect between Au NPs and AC towards the reduction of nitrophenols.

1. Introduction

Noble metal nanoparticles (MNPs) in catalytic applications have received significant interest because the nanoparticles possess unusual physiochemical properties with large number of exposed metal atoms, which greatly enhance the catalytic activity [1–5]. Gold nanoparticles (Au NPs) with features of high specific surface area, less prone to metal leaching and self-poisoning are one of the most inspiring developments in catalysis field [5–8]. Among all the Au NPs-catalyzed reaction, catalytic reduction of 4-nitrophenol (4-NP) to 4-aminophenol (4-AP) by $NaBH_4$ has been used widely as model reaction to test its catalytic activity, since 4-NP exhibits high toxicity and stability for a long time in water, causing harm to ecosystem [9–13]. And most importantly, the generated aminophenol is known to be an important intermediate chemical in many industries as well as easier to be mineralized and removed compared to the nitrophenols [14]. However, Au NPs suffer from serious stability problems such as aggregation in practice due to their high surface energy, eventually losing of their intrinsic activity [15–17]. In addition, considering facile catalyst recovery and recycling, immobilizing Au NPs on the surface of solid supports (e.g. silica, metal oxides and polymer) is regarded as an efficient approach for preventing aggregation of Au NPs and warranting high catalytic activity [18–21]. However, the stability of mentioned solid supports is compromised in some chemical environments of high or low pH solutions, resulting in the inability to achieve highly distributed Au NPs and dissolution of solid supports [22–24]. Thus, it is desirable to find a rational support with high stability to enhance the catalytic activity and efficiency of Au NPs.

Activated coke (AC), as a kind of carbon-based material, exhibits excellent properties with graphite-like layer crystallite and possesses appreciable environmental and economic benefits owing to its better mechanical strength, easier regeneration and lower cost compared with other carbon-based materials [25–27]. AC with mesopore and macropore structures can reduce the influence of internal diffusion on the general rate of adsorption and catalytic process greatly [22,28–30], which is different from microporous activated carbon. In addition, with

* Corresponding authors at: College of Environmental Science and Engineering, Hunan University, Changsha 410082, PR China.
E-mail addresses: zgming@hnu.edu.cn (G. Zeng), laicui@hnu.edu.cn (C. Lai).
[1] These authors contributed equally to this article.

https://doi.org/10.1016/j.apsusc.2018.12.207
Received 20 August 2018; Received in revised form 20 November 2018; Accepted 22 December 2018
Available online 24 December 2018
0169-4332/

abundant functional groups, AC could provide the active sites and is beneficial for MNPs anchoring and dispersion [31,32]. Moreover, AC possesses a graphite-like layer crystallite structure and flourishing hole structure, leading to high adsorption ability via π-π stacking interactions and thus facilitating the interface reaction with organic compounds, which could enhance the catalytic efficiency [33–35]. Therefore, AC can be considered as a promising, suitable and novel support, particularly, in catalytic applications.

To date, AC has been used as a carrier for supporting CuO-CeO_2, MnO_x-CeO_2 mixed oxides for fuel gas desulfurization, denitrification and mercury removal [31,36–38]. However, to the best of our knowledge, few papers thus far have reported on the utilization of MNPs decorated on AC and on their application of catalytic activity for organic transformation in wastewater treatment. In this regard, ideas of Au NPs supported on AC for the application in catalytic reaction of organic compounds are encouraged. The presence of abundant amount of oxygen-containing groups and thiol group endows its hydrophilic character and provides sufficient reactive sites for Au NPs anchoring, which is beneficial for catalytic reaction [28,39]. And, the good conductivity of AC can favor the electron transfer between Au NPs and AC [28]. It is well documented that electron transfer effect can conduce to negative shift in Fermi level of Au [16]. What's more, the utilization of AC as supports can expand its application in wastewater treatment in view of low cost of AC. On one hand, AC is able to prevent Au NPs from aggregation, warranting high catalytic activity. On the other hand, the synergistic effects between decorated Au NPs and AC were supposed to play the vital role in enhancing catalytic activity. Hence, using AC as a support for Au NPs anchoring seems to be a potential approach to fabricate a novel catalyst with enhanced catalytic activity for organic transformation in wastewater treatment.

Herein, taking full advantage of AC, we prepared Au/AC catalysts via a facile and one step method employed ascorbic acid as a mild reducing agent. The Au/AC catalysts were characterized by XRD, TEM, FTIR and XPS. The catalytic performance of Au/AC was investigated in the reduction of 4-NP in the presence of $NaBH_4$, with the rate constant evaluated in accordance with pseudo-first-order kinetic reaction under different Au loading amounts, catalyst dosage and $NaBH_4$ concentration. Besides, Au/AC was tested for the reduction of other nitrophenols such as 2-nitrophenol (2-NP), 2,4-dinitrophenol (2,4-DNP) and reductive degradation of azo dyes, including congo red (CR), methly orange (MO) and erichrome black T (EBT). The reusability of catalysts was tested up to six cycle run in the catalytic reduction of 4-NP. In addition, the feasible mechanism was discussed for the catalytic reduction of nitrophenols.

2. Experimental

2.1. Materials

Virgin activated coke (AC) used in the experiment is commercial cokes from Clear Science Technology Co., Ltd. (Shanghai, China). AC was washed with ultrapure water for several times and dried 12 h at 60 °C in an vacuum oven before grated with ball mill and sieved to 200 mesh size for further use. Hydrogen tetrachloroaurate hydrate ($HAuCl_4{\cdot}4H_2O$), sodium borohydride ($NaBH_4$), ascorbic acid (AA), 2-nitrophenol (2-NP), 4-nitrophenol (4-NP), 2,4-dinitrophenol (2,4-DNP), Methyl orange (MO) were purchased from Sinopharm Chemistry Reagent Co., Ltd. (Beijing, China). Congo red (CR) was purchased from Yuanhang chemical plant (Shanghai, China). Erichrome black T (EBT) was obtained from Shanpu Chemistry Reagent Co., Ltd. (Shanghai, China). All chemicals were of analytic reagent grade and used without further purification.

2.2. Preparation of Au/AC

Au/AC catalysts with different Au loading amount (1, 2, 3 mL of 1 wt% $HAuCl_4{\cdot}4H_2O$) were synthesized by a facile one-step method and labeled as Au/AC-x (x = 1, 2, 3), respectively. For the typical synthesis of Au/AC-1, 0.4 g of AC was added to 200 mL of ultrapure water under ultrasonicating for 0.5 h to obtain AC suspension. Then, 1 mL of $HAuCl_4{\cdot}4H_2O$ (24.28 mM) was added with stirring for 0.5 h. After that, 10 mL of ascorbic acid (0.1 M) was injected drop by drop into the above solution under stirring. Further, the reaction mixture was allowed for stirring for 24 h under ambient environment. The resulting black products were collected by filtration and washed with ultrapure water for several times, and then dried overnight at 35 °C in vacuum oven for further use. Similar synthetic procedure was applied for preparation of Au/AC-2 and Au/AC-3 catalysts with different Au loading amount.

2.3. Catalytic reduction of nitrophenols and azo dyes

The catalytic activity of as-prepared catalyst Au/AC for nitrophenols reduction in the presence of excess sodium borohydride was studied by UV–Vis spectrophotometer in a 3 mL quartz cuvette. In a typical procedure, 30 mL of 4-NP aqueous solution (0.2 mM) was taken in a cuvette followed by adding 15 mL of freshly-prepared $NaBH_4$ solution (0.1 M). Then, 9 mg of catalyst was added into the cuvette. 3 mL aliquots were collected followed by the solid-liquid separation, then the absorbance of samples was immediately monitored at different time intervals using a UV–Vis spectrophotometer in a scanning range of 200–800 nm. In addition, the catalytic reduction of 2-NP and 2,4-DNP were carried out following the same procedure. The similar procedure was applied for examining the performance on catalytic degradation of azo dyes (CR, MO and EBT). All the experiments were carried out under ambient experiment. The reusability of catalyst was examined via Au/AC separated by centrifugation after completely catalytic reduction of 4-NP in the first run.

2.4. Characterizations

UV–Vis spectrophotometer was recorded from 200 to 800 nm on a UV-2700 spectrophotometer (SHIMADZU (JAPAN) Co., Ltd.). The X-Ray diffraction (XRD) patterns were collected using a XRD-6100 powder diffractometer (SHIMADZU (JAPAN) Co., Ltd.). Transmission electron microscopy (TEM) and high-resolution TEM (HRTEM) were carried out using a transmission electron microscope Tecnai G2 F20 (FEI USA), attached with selected area electron diffraction (SAED) to observe the morphology and composition of the samples. Scanning transmission electron microscope with high-angle annular dark-field detector (HAADF-STEM) was used to record the elemental mappings. Fourier transform infrared spectroscopy (FT-IR) studies were conducted using FTIR-8400 S IRprestige-21 (SHIMADZU (JAPAN) Co., Ltd.), recorded from 4000–400 cm^{-1} at a resolution of 2 cm^{-1}. The X-ray photoelectron spectroscopy (XPS) measurements were performed on K-Alpha 1063 spectrometer (Thermo Fisher Scientific, UK). The Au loading amount was determined by inductively coupled plasma atomic emission spectrometry (ICP-OES, Perkin-Elmer Optima 5300DV, USA).

3. Results and discussion

3.1. Characterization of Au/AC catalyst

The XRD measurements were conducted to identify the phase purity and crystallite structure of virgin AC and as-prepared catalysts. As shown in Fig. 1, the characteristic diffraction peaks of AC appeared at 2θ = 26.66°, indicating AC possesses a graphite-like layer crystallite structure with hexagonal lattice [30]. The peak intensity at 26.66° decreased with increase of AC loading amount. The increase of Au loading amount may occupy more grain boundaries and affected the interplanar spacing of AC [31,40], thus leading to a decrease of crystalline quality of AC. The above results could also be inferred that the interaction may exist between Au and AC, as demonstrated as follows in TEM, FTIR and

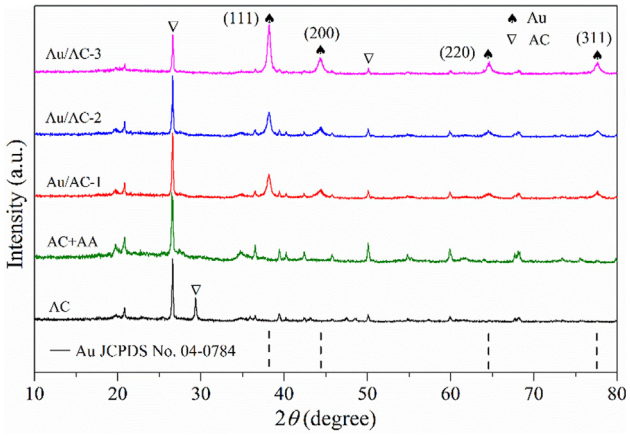

Fig. 1. X-ray diffraction patterns of virgin AC and Au/AC catalysts with different Au content.

XPS. What's more, the peak at nearly 29.4° corresponding to AC was also detected over virgin AC. Interestingly, compared with the virgin AC, the peak at 29.4° disappeared in XRD pattern of AC that reacted with AA only. This indicates the synthesis process has an influence on the crystallinity of activated coke. As reported by Costanzo et al., the oxidation or reduction of ascorbic acid would affect the hydrogen bonding of hydrogen and oxygen atom [41,42], thus resulting in a decrease of crystalline quality of AC. Besides, the minor peaks at 20.8°, 38.9° and 59.89° were ascribed to the presence of trace quantity of silica, aluminum and calcium as shown in Fig. S1B, which was corresponding with previous report that these elements were inert for the catalytic reaction [43]. In each pattern of catalyst with different Au loading amount, the crystallite structure of Au NPs was confirmed by the presence of diffraction peaks at 38.18°, 44.38°, 64.52°, and 77.54°, corresponding to the diffraction of the (1 1 1), (2 0 0), (2 2 0) and (3 1 1) lattice plane for Au(0) crystals, respectively (JCPDS NO. 04-0784). The XRD patterns of catalysts matched the face-centered-cubic (fcc) nature of Au NPs [16]. With the increment of Au loading amounts, the intensity of scattering peaks heightened, which could be attributed to the growth and formation of larger Au NPs as the Au loading amounts increasing [16].

In order to study the morphology and microstructure of the virgin AC and obtained Au/AC, TEM measurements were performed (Fig. 2). By the morphology image of virgin AC as indicated in Fig. 2A, it is clear that virgin AC contains some wrinkles composed by some thin layers with relatively smooth and planar surfaces. As revealed from Fig. 2B, the Au NPs were dispersed uniformly on the stacking AC layers. From Fig. 2C and D, it could be observed that Au NPs with a size smaller than 5 nm existed in AC, with interplanar spacing of 0.235 nm corresponding to the (1 1 1) crystal planes. This was because the pore structure of AC restricted the growing of Au NPs adsorbed into the AC. As shown in Fig. 2E, HRTEM image reveals distinct lattice fringes with an interplanar spacing measured to be 0.235 nm and 0.205 nm, corresponding to the (1 1 1) and (2 0 0) crystal planes of fcc Au, respectively. Moreover, the SAED pattern was inserted in Fig. 2E, displaying the characteristic rings for the (1 1 1), (2 0 0), (2 2 0) and (3 1 1) planes of fcc Au. Both results confirm the polycrystalline structure of Au NPs supported on AC and are in good accordance with the XRD results. Besides, the SEM images of Au/AC-3 in Fig. S2A further displayed that there were Au NPs dispersed on the surface of AC. Base on the Figs. 2C, D, S2B and C, the particle size of Au NPs supported on AC was counted for at least 200 nanoparticles, which would make the size distributions more representative and accurate. Fig. 2F shows the presence of dispersed Au NPs with a diameter of 14.9 ± 10.8 nm. In addition, to further confirm the elemental distribution and chemical composition of Au/AC-3, HAADF-STEM image and EDS spectrum were carried out (Fig. S1). The HAADF-STEM image shows a clear luminance of Au NPs, revealing homogenous distribution of Au NPs on AC. The presence of Au element confirmed the synthesis of Au NPs. These TEM images further indicate the successful preparation of Au NPs supported on AC as well, and illustrate Au NPs dispersed well on AC surface.

FTIR measurements were performed to further obtain valid information of functional group about virgin AC and Au/AC-3 catalyst. In the region of 3600–3200 cm^{-1}, the most pronounced broad and intense band around 3421 cm^{-1} was due to the overlapping of −OH as exhibited in the FTIR spectrum of activated carbon or a displaced amino group [38,44]. And the band located at 2362 cm^{-1} was assigned to the vibration of C═O [45]. The peaks at 1635 and 1445 cm^{-1} corresponded to the skeletal vibrations stretching of aromatic C═C [19]. The peak at 1037 cm^{-1} represented a stretching vibration of C−O or primary alcohols[46]. In addition, the peaks at 670–872 cm^{-1} represented out of plane bending vibrations of the C−H bonds [38]. It can be seen from the FTIR spectrum of Au/AC-3 that after the deposition with Au NPs on AC, some adsorption peaks drifted, appeared and disappeared. The attenuated peaks at 3421 and 1445 cm^{-1} indicated that the amount of O−H bonds decreased after active sites of AC were occupied by Au NPs. In addition, the shift of the band at 2626, 2362 and 1635 cm^{-1} may be accounted for the interaction of Au NPs with hydroxyl groups of AC [47]. The gradual variation in this band region of 900–700 cm^{-1} was owing to Au−O bonds stretching vibration. These variation and vibration indicated the reduction of oxygen-containing groups [48]. However, on account of the weak dipoles exhibited by S-H groups, the thiol group in FTIR is invisible under current conditions [49]. Fig. 3 indicates that the surface functional groups in AC contain oxygen-containing functional groups such as hydroxyl and carboxyl, possessing hydrophilic property in solvents which may favor catalytic reaction [39,50].

The XPS was employed to further analyze the composition and surface-functional groups of prepared catalysts. As shown in Fig. 4A, the binding energies (BE) of about 530, 284 and 163 eV indexed to O 1s, C 1s and S 2p, respectively. As shown in Fig. 4B, in the high-resolution XPS spectrum of Au 4f region, the peaks of Au $4f_{7/2}$ an Au $4f_{5/2}$ peaks were observed at 84.2 and 87.9 eV respectively, with a gap of 3.7 eV between two peaks [51]. It should be noted that the typical characteristic peaks of Au(III) were absent in the spectrum, illustrating the almost completed reduction of the small amount of Au(III) to Au(0) in the reaction system [51]. The O 1s spectra of Au/AC-3 and AC are shown in Fig. 4C. The photoelectron line of about 531.8 and 532.9 eV were attributed to oxygen in carboxylate/carbonyl (O−C═O/C═O) and in the epoxy/hydroxyl (C−OH) of the AC [52,53]. It has been found that the shifting BE of O 1s ascribed to O−C═O/C═O and C−OH were occupied by Au NPs, revealing the oxygenated functional group like hydroxyl were reduced during the preparation of catalysts, and Au NPs occupied the sites of these functional groups [54]. The claim was further verified by the C 1s spectra of Au/AC-3 and AC in Fig. 4D. The C 1s spectra could be deconvoluted into five components corresponding to sp^2 carbon (284.6 eV), −CONH (285.1 eV), C−O−C (286.6 eV), C═O (287.7 eV) and O−C═O (288.8 eV) [28,46,54,55]. They were attributed to the presence of carboxylate, carbonyl and hydroxyl functional groups of AC. Obviously, after AC loaded with Au NPs, the peak intensity of oxygenated functional groups (C−C, C═O) decreased (Table S1), which was assigned to the formation of Au NPs on these functional groups [48]. The peak of C-O-C showed a slight shift compared with the virgin AC, owing to the galvanic displacement reaction between catechol groups and Au NPs [56]. Thus, the XPS measurements validate the presence of sulfur-containing and oxygen-containing groups in AC surface.

3.2. Catalytic reduction studies of nitrophenols

Before checking out the catalytic nature of synthesized catalysts Au/AC, it has to check whether self-hydrolysis of $NaBH_4$ reduces the 4-NP

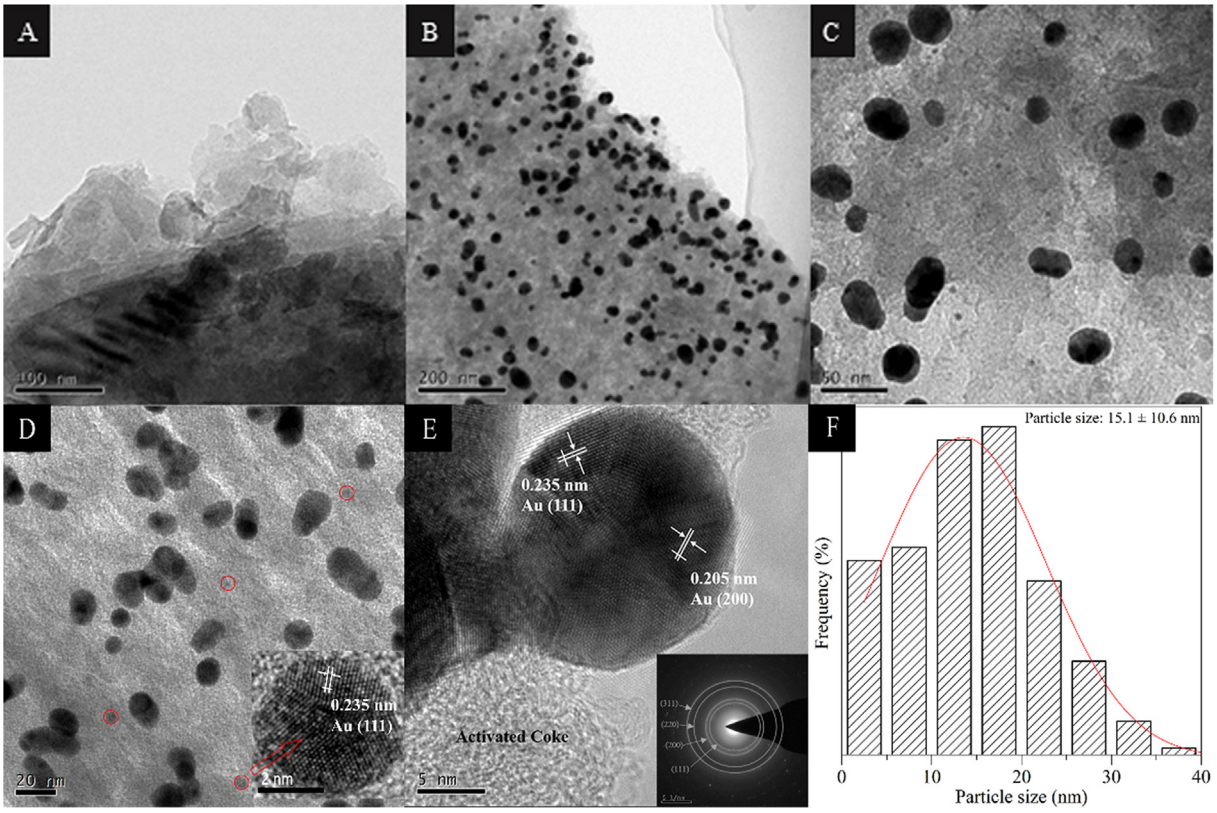

Fig. 2. TEM images of virgin AC (A) and the Au/AC-3 catalyst (B–D) (the inset is HRTEM image of the tiny NPs); HRTEM image (E) of Au/AC-3 catalyst (the inset is SAED pattern); Size distribution of Au NPs (F).

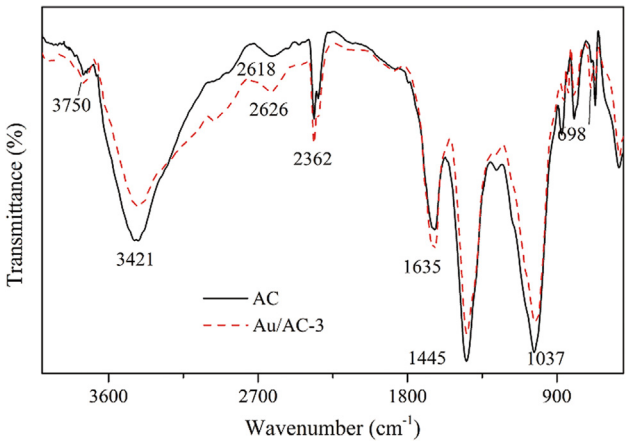

Fig. 3. FTIR spectra of AC and Au/AC-3 catalyst.

and the support material AC catalyzes the reduction of 4-NP. For these reason, two control experiments were performed in which the reductions of 4-NP were investigated in the presence of $NaBH_4$ and AC + $NaBH_4$. After the additional of $NaBH_4$ in the 4-NP, the color of the mixture aqueous turned to bright yellow rapidly, indicating the 4-NP was converted into nitrophenolate anion ($C_6H_4NO_3^-$). As shown in Fig. S3, the initial maximum absorbance at 400 nm indexed to the 4-NP in the natural and alkaline conditions. The maximum absorbance peak of the mixture solution centered at 400 nm over reaction time within 20 min in the absence of catalyst wherein excess $NaBH_4$ was used exclusively, indicating the reduction does not occur by the self-hydrolysis of $NaBH_4$ [57]. This can be ascribed to that there is a kinetic negative barrier and mutual repulsion between BH_4^- and 4-NP [58]. On the other hand, the absorbance peak at 400 nm also decreased slightly within 20 min but no peak appeared at 298 nm in the control experiment in the presence of virgin AC + $NaBH_4$, indicating the catalytic reaction did not proceed at all and AC has adsorption ability towards 4-NP. Nevertheless, it should be point out the adsorption efficiency is modest. Thus, the adsorption effects of AC towards nitrophenols can be ignored.

In order to study the catalytic performance of synthesized catalyst, catalytic reduction of 4-nitreophenol in the presence of excess sodium borohydride was carried out. The convincing evidence for reduction of 4-NP came from time-dependent UV–Vis absorption spectra. Fig. 5A provides time-dependent UV–Vis absorption spectra of 4-NP catalyzed by 9 mg of Au/AC-3. The absorbance peak at 400 nm quickly decreased and disappeared within 20 s. Simultaneously, a new peak appeared at 298 nm, accompanied with an increase intensity of the peak over reaction time, which was assigned to the formation of 4-aminophenol. In order to confirm the product, the determination of 4-AP was recorded with UV–Vis absorbance spectra (Fig. 5B). Moreover, the isosbestic points at 313 nm also provided evidence to the catalytic reduction of 4-NP yields 4-AP without any byproduct [59]. As the initial concentration of $NaBH_4$ (0.1 M) was excess with respect to the concentration of 4-NP (0.2 mM), the reduction can be treated as pseudo-first-kinetic. The reduction rate of 4-nitrophenol was calculated using the following equation:

$$-\ln(C_t/C_0) = -\ln(A_t/A_0) = k_{app}$$

wherein C_t is 4-NP concentration at reaction time *t*, and C_0 is the initial concentration of 4-NP, and the rate constant k_{app} is the first order constant, determined by a liner plot of $\ln(C_t/C_0)$ versus reaction time. Liner relationships between $\ln(C_t/C_0)$ and reaction time t was shown in Fig. 5A, and the rate constant k_{app} was calculated as 0.1916 s^{-1} for the reaction. As presented in Table 1, it is obvious that the catalytic performance of Au/AC-3 was comparable or even superior when compared with other Au-based catalysts supported by other materials. It is well documented that the high catalytic activity of Au NPs is owing to their

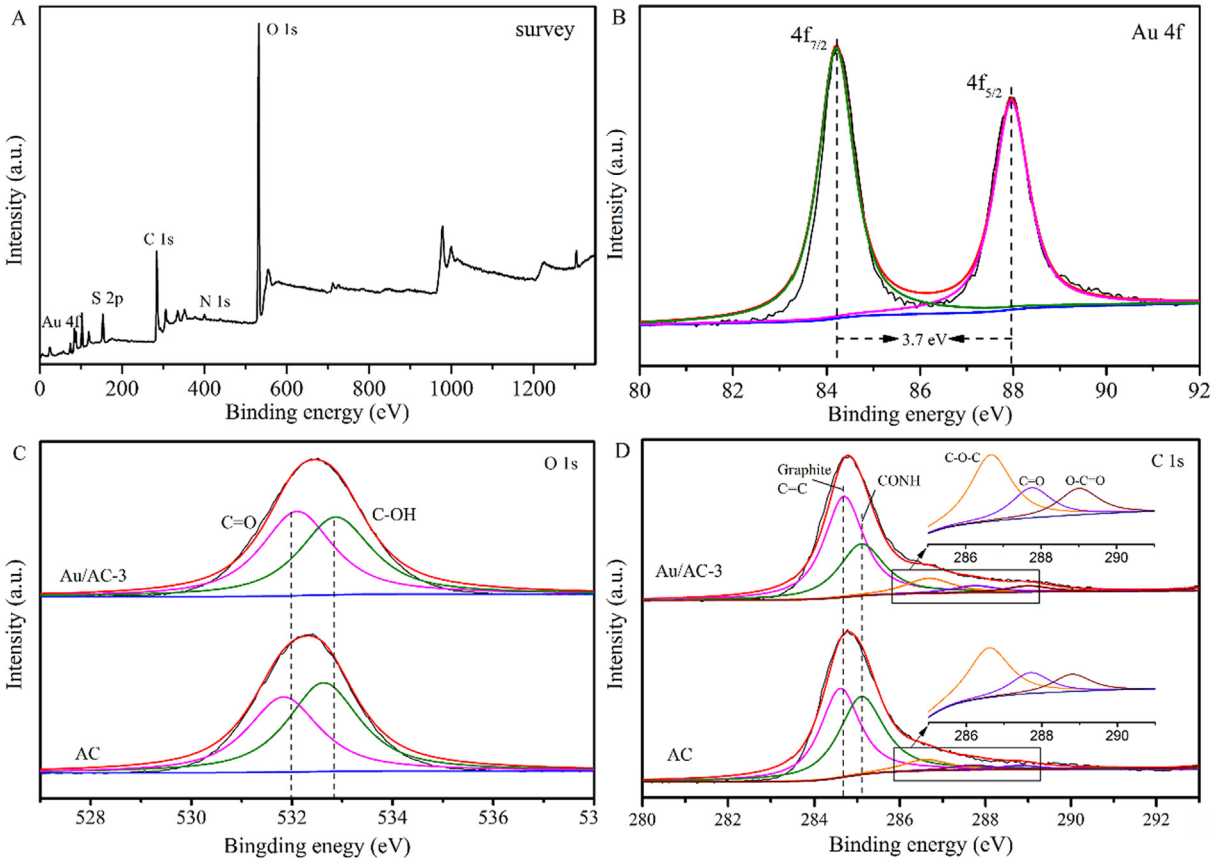

Fig. 4. XPS survey spectra (A) of Au/AC-3 catalyst; High-resolution XPS spectra of Au 4f (B), O1s (C) and C 1s (D) of Au/AC-3 and AC.

highly dispersed and nanosized properties, which is corresponding to the above characterization of Au/AC. In the cases of other loading amounts of the Au catalysts, the catalytic reduction of 4-NP was performed under similar conditions. The catalytic reduction of 4-NP completed within 50, 30 and 20 s, respectively. For apparent comparison of rate constant k_{app} of different Au loading amounts catalysts, the C/C_0 and ln (C/C_0) versus reaction time were plotted in Fig. 6A and B. The rate constant k_{app} was 0.0737, 0.1347, and 0.1916 s^{-1}, respectively. As expected, the rate constant k_{app} was proportional to the concentration of the $HAuCl_4$ solutions, indicating that the catalytic efficiency increased with the increased loading amounts of Au NPs on AC. It is obviously shown in Fig. S4 that with the lower Au loading amounts, the sparse distribution of Au NPs resulted in the low catalytic activity. In Au/AC-3 catalyst, Au NPs were well dispersed on AC, with the better surface morphology, which relates to the higher catalytic activity. This result is in well consistent with previous studies, demonstrating that the catalytic activity is proportional to the quantity of nanoparticles [60]. Furthermore, the Au content determined by ICP-OES was about 1.37 wt %, 2.45 wt% and 3.49 wt%, corresponding to Au/AC-1, Au/AC-2 and Au/AC-3, respectively. According to the previous research, the turnover frequency (TOF: moles of 4-NP reduced by per gram of Au NPs per second) has been calculated to estimate the catalytic efficiency of catalysts in our research [61,62]. TOF was calculated to be 0.287, 0.268 and 0.282 $mol \cdot g^{-1} \cdot s^{-1}$, for the case of Au/AC-1, Au/AC-2 and Au/AC-3, respectively. It is higher than those of Au NPs catalysts recently reported. Thus we have a workable and efficient Au/AC catalyst with

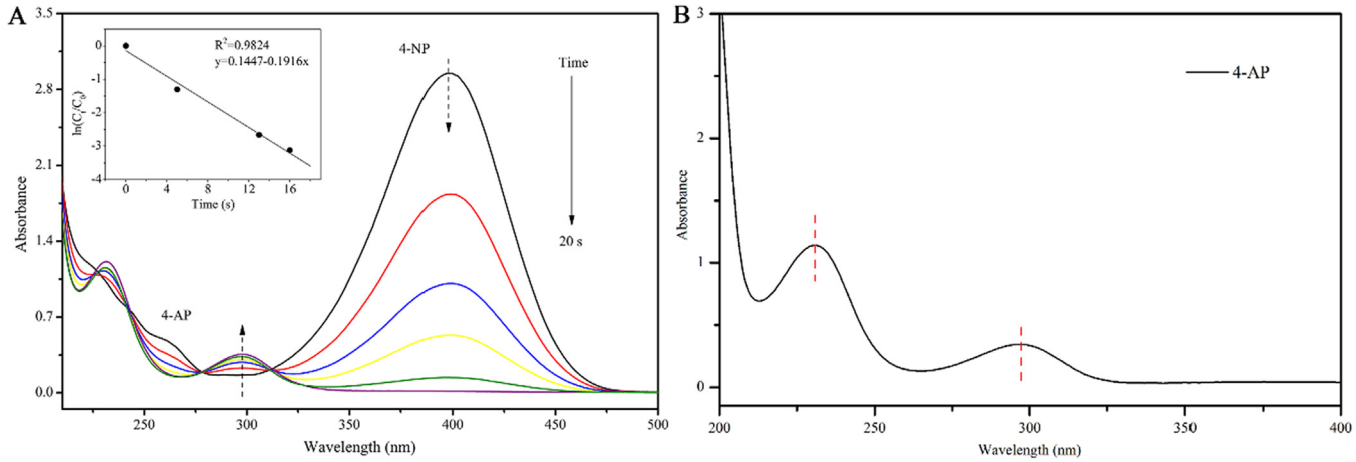

Fig. 5. Time-dependent UV–Vis absorption spectra of the reduction of 4-NP catalyzed by Au/AC-3 (A) and plot of ln(C/C_0) versus the reaction time (B).

Table 1
Compaision of the catalytic performances of Au/AC with the reported AuNPs catalysts supported on orther materials for the reduction of 4-NP.

Catalysts	Supported materials	Catalyst dosage (mg)	Time (s)	k_{app} (10^{-3} s^{-1})	k_{nor} (s^{-1} g^{-1})	Ref.
Au/AC[a]	Activated coke	9	20	191.6	21.3	This work
Au_3-Cu_1/rGO[b]	Graphene Oxide	0.1	30	96	960	[63]
Ag-Au-rGO[b]	Reduced grapheme oxide	0.1	360	3.47	34.7	[6]
Au/GO[c]	Graphene Oxide	–	45	107.97	–	[64]
GO-Fe_3O_4[d]-Au NPs	Graphene Oxide	0.02	100	0.322	16.1	[19]
Au@CMK-3-O[e]	Mesoporous carbon	75	300	7.75	0.103	[65]
Au/g-C_3N_4[f]	g-C_3N_4	1	600	5.936	5.936	[16]
CNFs[g]@Au core–shell network	Carbon nanofibers	0.1	300	5.42	54.2	[66]
Au@PZS@CNTs[h]	Carbon nanotubes	0.3	960	1.78	5.93	[67]
AuNPs/Chitosan	Chitosan	50	67	0.561	0.011	[61]
Au/MgO[i]	magnesium oxide	15	150	7.6	0.507	[68]

[a] AC, activated coke.
[b] rGO, reduced graphene oxide.
[c] GO, graphene oxide.
[d] GO-Fe_3O_4, graphene oxide–Fe_3O_4 nanocomposite.
[e] CMK-3-O, oxidized mesoporous carbon.
[f] g-C_3N_4, Graphitic carbon nitride.
[g] CNFs, carbon nanofibers.
[h] PZS@CNTs, polyphosphazene functionalized carbon nanotubes.
[i] MgO, magnesium oxide. k_{nor}, the rate constant normalized with the catalyst dosage (k_{app}/the mass of catalyst, s^{-1} g^{-1})

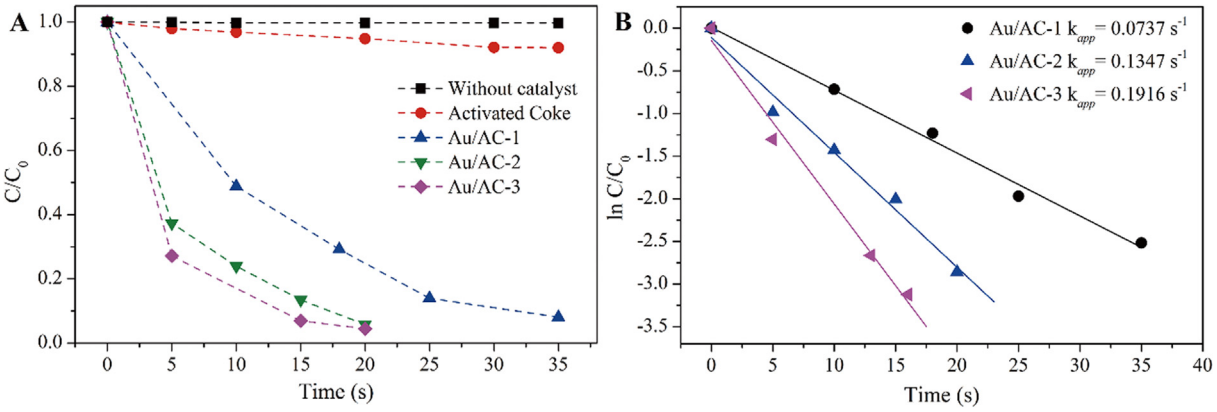

Fig. 6. C_t/C_0 (A) and $\ln(C_t/C_0)$ (B) versus the reaction time for the reduction of 4-NP catalyzed by different Au loading amounts catalysts, respectively.

relatively high TOF, which is important to the value of a catalyst in industrial applications.

According to the Sabatier principle, the interaction between substrate and catalyst should be optimum with regard to the higher catalytic activity [69]. Thus, the effect of the catalyst dosage on the reduction of 4-NP was also investigated under identical conditions. It can be seen from Fig. 7A, the rate constant k_{app} increased intensively with the catalyst dosage increasing until the catalyst dosage was 9 mg. This can be ascribed to the more availability site of active catalytic surfaces with the increase in catalyst dosage [70]. However, the rate constant k_{app} increased slowly as the catalyst dosage increased from 9 to 12 mg. When the dosage was over 9 mg and reached 12 mg, the increasing amount of rate constant k_{app} was very small, from 0.1916 to 0.2210 s^{-1}. This could be ascribed to that the reactants were saturated that even more availability sites of active catalytic surfaces could not further enhance the reaction rate at the same initial concentration of 4-NP [71].

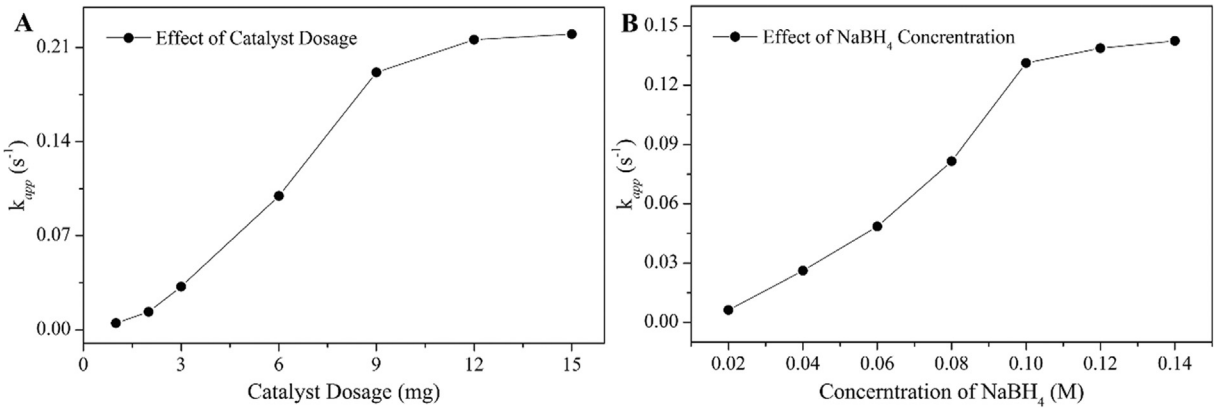

Fig. 7. The effect of catalyst dosage (A) and $NaBH_4$ concentration (B) on the catalytic reduction of 4-NP catalyzed by Au/AC-3.

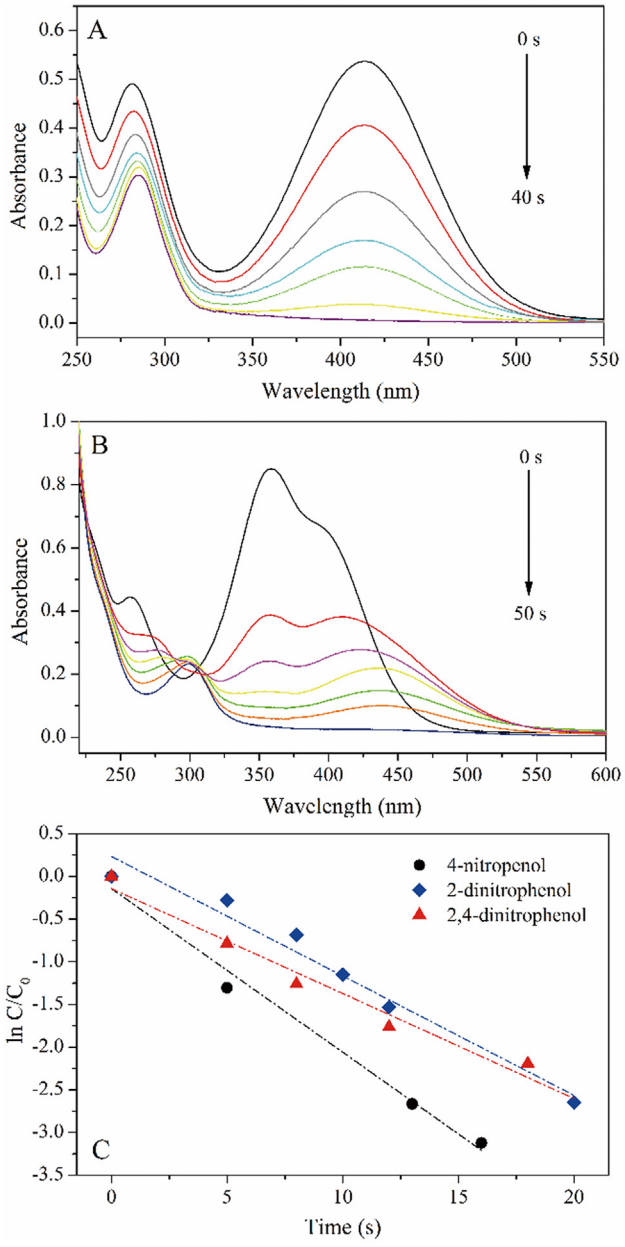

Fig. 8. Time-dependent UV–Vis absorption spectra of the reduction of 2-NP (A) and 2,4-DNP (B) and $\ln(C_t/C_0)$ versus the reaction time (C) for the reduction of 4-NP, 2-NP and 2,4-DNP catalyzed by Au/AC-3, respectively.

For the balance of the highest rate and minimum catalyst dosage in the concept of economic friendly, the catalyst dosage of 9 mg was used with the current experimental conditions. Moreover, the study of the optimization of the $NaBH_4$ concentration was also investigated. With the initial $NaBH_4$ concentration increasing, the concentration of nitrophenolate anion increased (Fig. S5). Similarly, the catalytic efficiency of Au/AC catalysts tends to increase upon addition of more $NaBH_4$. Fig. 7B shows that the rate constant k_{app} increased intensively by increasing the $NaBH_4$ concentration, and increased slowly after the $NaBH_4$ concentration of 0.10 M. Therefore, the optimum $NaBH_4$ concentration was 0.10 M for the catalytic reduction in the study.

Furthermore, the catalytic reduction of other nitrophenols (2-NP and 2,4-DNP) was investigated to confirm the catalytic activity. The time-dependent UV–Vis absorption spectra of 2-NP and 2,4-DNP is presented in Fig. 8A and B. In natural and alkaline conditions, the distinct bands of 2-NP and 2,4-DNP were 415 and 359 nm, respectively

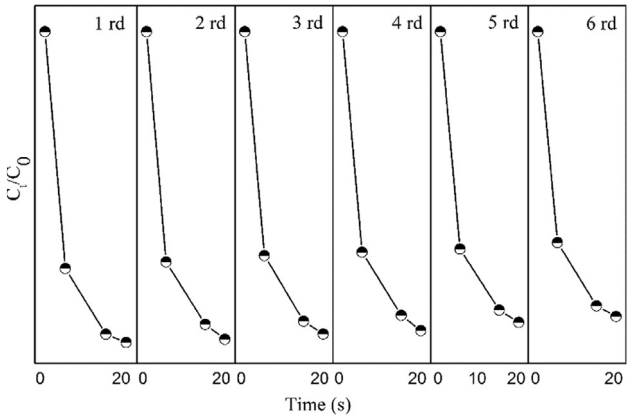

Fig. 9. Six cycling reduction curves of 4-NP catalyzed by Au/AC-3 in the presence of $NaBH_4$.

[72]. Then, the intensity of their absorbance peak gradually decreased within 40 s and 50 s, accompanied with decolorization upon the additional of Au/AC-3 catalysts. As shown in Fig. 8C, we found that Au/AC-3 exhibited high catalytic activity with excellent yields towards other nitrophenols regardless of the position of the substituents. When the reduction of 4-NP, 2-NP and 2,4-DNP was catalyzed by Au/AC-3, the rate constant k_{app} was 0.1916, 0.1399 and 0.1229 s^{-1}, respectively. It can be concluded that the catalytic activity of reduction of 4-NP showed a better activity than that of 2-NP and 2,4-DNP, which may related to the substituent positions [73]. Nonetheless, the Au/AC catalyst exhibits magnificent catalytic activity towards various nitrophenols.

The reusability of the catalyst was also investigated with the reduction of 4-NP. After completely catalytic reduction of 4-NP in the first run, the Au/AC could be easily separated by centrifugation from reaction solution, and then washed three times and dried for the further use in next cycle of the reduction of 4-NP. As shown in Fig. 9, the conversion of 4-NP to 4-AP was 84% in 20 s after six cycles. Thus, the Au/AC still exhibited good catalytic activity after six cycles without significant loss of active sites, owing to the supporting effect of AC. It should be noted that although novel catalyst with superior catalytic performance has been developed, the method for addressing the problem of weight loss after each cycles and higher catalytic activity should be focused on further study. Hence, more experiments will be carried out to address above issues in our further research.

3.3. Feasible mechanism for reduction of nitrophenols

It has been widely accepted that the catalytic reduction of nitrophenols in the presence of $NaBH_4$ obeys the classical Langmuir-Hinshelwood model on account of the surface catalysis of catalytic reduction reactions [74]. Based on the experimental data, a feasible mechanism for the reduction of nitrophenols catalyzed by Au/AC was proposed in Scheme 1: (i) BH_4^- is adsorbed on to the catalytic surface, then generating BO_2- by the self-hydrolysis of $NaBH_4$. Meanwhile, BH_4^- reacts with Au NPs, transferring active hydrogen species to form the active surface-hydrogen Au-H [69,75]. (ii) From Fig. 5, it can be speculated that there is an induce time for 4-NP adsorption, which is in good agreement with the results that the concentration of 4-NP decreased at the initial but the concentration of 4-AP was no significant increase. Thus, 4-NP would adhere reversibly to the surface of Au/AC owing to the adsorption of AC [75]. Simultaneously, the active surface-hydrogen transfers to the nitro groups $-NO_2$, attacking $-NO_2$ to reduce to form corresponding amino groups with the electron transferring from BH_4^- to $-NO_2$ [19]. It has been reported that the catalytic reduction is owing to electron transfer between the $NaBH_4$ and the $-NO_2$ when there is direct contact between the Au NPs and $-NO_2$ [19,76]. (iii) The generated aminophenol compounds were desorbed from the surface of

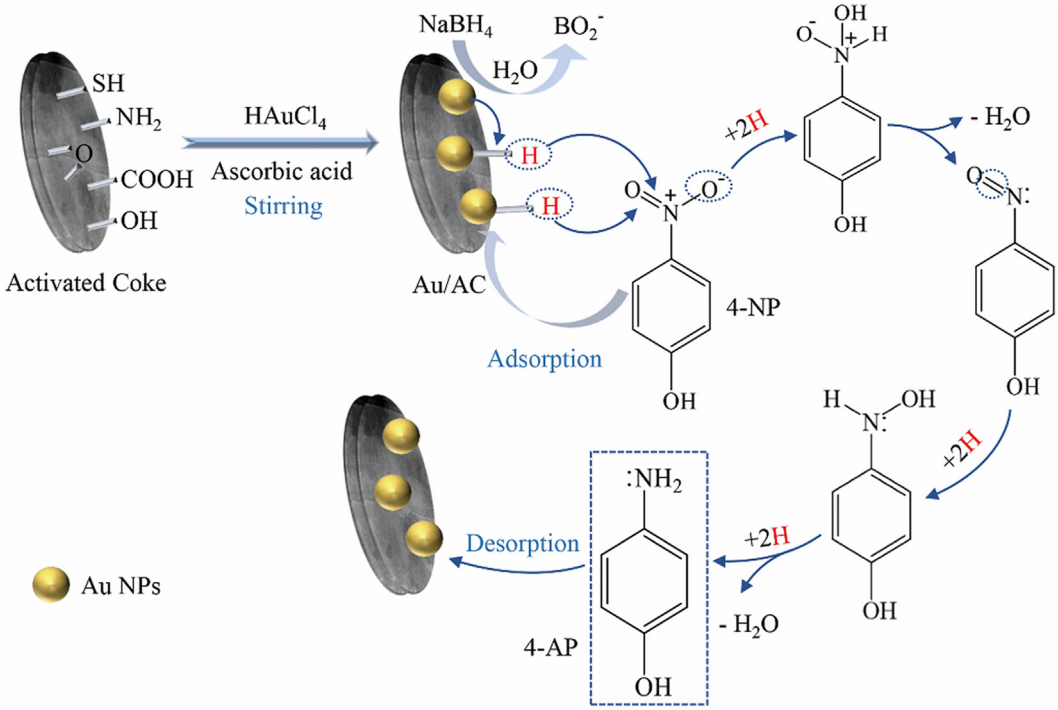

Scheme 1. Possible mechanism of catalyst preparation and catalytic reduction of 4-NP.

Au/AC.

In summary, it can be concluded that Au/AC exhibits high catalytic activity towards the reduction of nitrophenols, which can be postulated that such high catalytic activity of Au/AC is ascribed to these factors: (1) It has been well documented that Au NPs can be easily bonded to the sulfur atom on the surface of AC [49], guaranteeing the relative tight combination of Au NPs and AC. Besides, with electron-rich feature of other abundant oxygen-containing groups, the AC as support is in favor to anchor and disperse Au NPs firmly through complexing or electrostatic interaction, which is vital in using metal nanoparticles catalyst in organic transformation [28,46,64]. (2) AC can promote the adsorption of reactants, which provides a higher concentration of nitrophenols near to Au NPs on AC. This could provide more opportunity for nitrophenols molecules to expose onto active sites of the catalysts and thus accelerate the reaction kinetics [28,64]. (3) AC possesses a graphite-like layer crystallite structure, which is beneficial for the adsorption of 4-NP via π-π stacking interactions. This can shorten the distance between 4-NP and Au NPs supported on AC. Besides, the electrical conductivity of AC is in favor of the electron transfer during reaction. (4) Previous research has shown that the high catalytic activity also can be attributed to the use of a weakly binding agent ascorbic acid in the synthesis and the large defect to volume ratio of the Au NPs [77,78]. Furthermore, the nanosized Au NPs with a higher redox potential value, are beneficial for accelerating the electron transfer in the catalytic system and consequently lower the kinetic negative barrier for the reduction [61]. It is concluded that the well-dispersed and nanosized Au NPs, the synergistic effects of the good adsorption capacity and electrical conductivity of AC as well as large defect to volume ratio may be responsible for the high catalytic performance of the Au/AC catalysts.

3.4. Degradation of azo dyes

Azo dyes, as a kind of toxic and hard-biodegraded industrial pollutant containing one or more azo bonds (−N═N−), are hazardous to environment at low concentrations and carcinogenic to human [79,80]. Thus, we extended the Au/AC catalysts to catalytic degradation of azo dyes to further investigate the catalytic performance of Au/AC. In this study, three kinds of azo dyes including CR, EBT and MO have been chosen as substrates. All the catalytic conditions of these azo dyes were same to that of 4-NP and the convincing evidence for degradation of azo dyes came from time-dependent UV–Vis absorption spectra.

As shown in Fig. S6, the initial maximum absorbance of CR, EBT and MO was at 495, 526 and 465 nm [81]. After the as-prepared Au/AC-3 was tried on CR, EBT and MO adsorption, the characteristic peaks in the corresponding UV–Vis spectra of CR, EBT and MO decreased within initial 15 min (Fig. S6A, C and E). With continuously stirring for another 15 min, these solutions achieved the adsorption equilibrium, with the adsorption efficiency of 30%, 35% and 12% for CR, EBT and MO, respectively. Especially, the adsorption efficiency of MO by Au/AC-3 was 32% at first 15 min and then decreased to 12% until equilibrium was achieved. Besides, the BET surface area (S_{BET}), pore volume, and average pore size of Au/AC-3 were determined to be 21.383 $m^2 g^{-1}$, 0.0938 $cm^3 g^{-1}$ and 17.55 nm (Table S2). It validates that Au/AC-3 possesses low adsorption ability [82].

Then, the reductant $NaBH_4$ was added to the above solution for triggering the catalytic degradation. As we can see from Fig. S6B, the characteristic peaks at 344 and 495 nm ascribed to the CR decreased rapidly over reaction time. However, a new peak at 250 nm occurred with the decolorization of solutions within several seconds (Fig. S7). After reaction, there was almost no absorbance at 344 and 495 nm, and the absorbance at 250 nm was maximized, confirming that the removal of CR and the formation of intermediates were caused by catalytic degradation [83]. Similarly, the characteristic peaks of EBT and MO disappeared accompanied with the decolorization within several seconds after adding the Au/AC-3 catalysts (Fig. S7), while the new peaks at 240 and 258 nm were emerged corresponding to the produced intermediates of EBT and MO (Fig. S6D and E) [84,85].

To sum up, the characteristic peaks of azo dyes decreased and the color of these solutions was decolorization during the reaction. Besides, new peaks were formed in the UV- range, suggesting azo dyes was indeed degraded, instead of just being absorbed by Au/AC-3 and the −N═N− bonds of azo dyes was broken down by Au/AC-3 [84]. The emerging absorption at about 250 nm appeared simultaneously with

−N=N− cleavage, indicating that there were newly produced colorless compounds [71]. These peaks were originated from the absorption from aromatic intermediates, which may ascribed to the two sides of the cleavage azo bond or their derivatives, corresponding to the results in previous reports [83,84]. Thus, the most of azo dyes were removed by the catalytic degradation by Au/AC-3. As is well-known, adsorption process can play a critical role on the removal of pollutants, including catalysis [19]. Compared with other study of catalytic degradation of azo dyes, the reductive degradation efficiency of Au/AC catalyst is obviously superior to that of other catalysts (Table S3). These results confirm the high reductive degradation activity towards various azo dyes of our catalyst. However, as shown in Fig. S8 the catalytic efficiency was different for the three azo dyes with the rate constant k_{app} followed the order by MO ($0.1863\,s^{-1}$) > EBT ($0.1197\,s^{-1}$) > CR ($0.0692\,s^{-1}$), attributed to the molecular formula and size, as well as the electrical feature of dyes [86]. The structural formulas of these dyes are given in Fig. S7, it can be concluded that with the fewer azo bonds and simpler molecular, the azo dyes could be degraded more easily. The structural formula of MO and EBT possesses single azo bonds, while CR contains a couple of azo bonds, causing that MO was reductive degraded more easily within 30 s. A speculated reason is that the less steric hindrance of dyes with the simpler molecular structural and easier electrostatic attraction between catalyst and dyes can promote these dyes to expose on the catalytic active sites, thus accelerating the catalytic degradation [86].

4. Conclusions

In this study, a facile one-step method was developed to prepare a novel Au/AC catalyst. Au NPs with a diameter of 16 ± 6 nm were supported on the surface of AC. The Au/AC catalyst exhibited excellent catalytic performance for the reduction of 4-NP with the rate constant k_{app} of $0.1916\,s^{-1}$. The catalyst also manifested remarkable catalytic activity for the reduction of other nitrophenols and degradation of azo dyes. It was found that the catalytic performance was comparable or even superior to that of some other Au-based catalyst. This could be attributed to the abundant oxygen-containing functional groups and thiol groups on the surface of AC, promoting the Au NPs firmly anchored and dispersed on AC. The AC in this study is an excellent supporting material and beneficial for the catalytic reaction. In addition, the synergistic effect of nanosized Au NPs, the good adsorption capacity of AC and large defect to volume ratio could enhance the catalytic activity. The catalyst exhibited good stability and the catalytic performance remained 84% over six recycles. Considering the low cost of AC, facile preparation method and excellent catalytic performance, Au/AC catalysts seem to have potential to serve as an efficient catalyst for the reduction of nitrophenols and azo dyes, as a pretreatment for wastewater treatment in diversified applications.

Conflicts of interest

There are no conflicts to declare.

Acknowledgements

This study was financially supported by the Program for the National Natural Science Foundation of China (51579098, 51879101, 51779090, 51709101, 51278176, 51408206, 51521006, 51809090, 51378190), Science and Technology Plan Project of Hunan Province (2018SK20410, 2017SK2243, 2016RS3026), the National Program for Support of Top-Notch Young Professionals of China (2014), the Program for New Century Excellent Talents in University (NCET-13-0186), the Program for Changjiang Scholars and Innovative Research Team in University (IRT-13R17), and the Fundamental Research Funds for the Central Universities (531109200027, 531107050978, 531107051080). Hunan Provincial Innovation Foundation for Postgraduate (CX2018B155).

Appendix A. Supplementary material

Supplementary data to this article can be found online at https://doi.org/10.1016/j.apsusc.2018.12.207.

References

[1] R. Ciriminna, E. Falletta, C. Della Pina, J.H. Teles, M. Pagliaro, Industrial Applications of Gold Catalysis, Angewa. Chem. Int. Ed. 55 (2016) 14210–14217.
[2] H. Mou, C. Song, Y. Zhou, B. Zhang, D. Wang, Design and synthesis of porous Ag/ZnO nanosheets assemblies as super photocatalysts for enhanced visible-light degradation of 4-nitrophenol and hydrogen evolution, Appl. Catal. B: Environ. 221 (2018) 565–573.
[3] C. Lai, X. Liu, L. Qin, C. Zhang, G. Zeng, D. Huang, M. Cheng, P. Xu, H. Yi, D. Huang, Chitosan-wrapped gold nanoparticles for hydrogen-bonding recognition and colorimetric determination of the antibiotic kanamycin, Microchim. Acta 184 (2017) 2097–2105.
[4] P. Xu, G.M. Zeng, D.L. Huang, C.L. Feng, S. Hu, M.H. Zhao, C. Lai, Z. Wei, C. Huang, G.X. Xie, Z.F. Liu, Use of iron oxide nanomaterials in wastewater treatment: a review, Sci. Total Environ. 424 (2012) 1–10.
[5] O. Ramirez, S. Bonardd, C. Saldias, D. Radic, A. Leiva, Biobased chitosan nanocomposite films containing gold nanoparticles: obtainment, characterization, and catalytic activity assessment, ACS Appl. Mater. Interfaces 9 (2017) 16561–16570.
[6] K. Hareesh, R.P. Joshi, D.V. Sunitha, V.N. Bhoraskar, S.D. Dhole, Anchoring of Ag-Au alloy nanoparticles on reduced graphene oxide sheets for the reduction of 4-nitrophenol, Appl. Surf. Sci. 389 (2016) 1050–1055.
[7] A. Balanta, C. Godard, C. Claver, Pd nanoparticles for C-C coupling reactions, Chem. Soc. Rev. 40 (2011) 4973–4985.
[8] L. Qin, G. Zeng, C. Lai, D. Huang, P. Xu, C. Zhang, M. Cheng, X. Liu, S. Liu, B. Li, H. Yi, "Gold rush" in modern science: fabrication strategies and typical advanced applications of gold nanoparticles in sensing, Coord. Chem. Rev. 359 (2018) 1–31.
[9] X. Ren, G. Zeng, L. Tang, J. Wang, J. Wan, Y. Liu, J. Yu, H. Yi, S. Ye, R. Deng, Sorption, transport and biodegradation – an insight into bioavailability of persistent organic pollutants in soil, Sci. Total Environ. 610–611 (2018) 1154–1163.
[10] C. Zhang, C. Lai, G. Zeng, D. Huang, C. Yang, Y. Wang, Y. Zhou, M. Cheng, Efficacy of carbonaceous nanocomposites for sorbing ionizable antibiotic sulfamethazine from aqueous solution, Water Res. 95 (2016) 103–112.
[11] F. Long, J.-L. Gong, G.-M. Zeng, L. Chen, X.-Y. Wang, J.-H. Deng, Q.-Y. Niu, H.-Y. Zhang, X.-R. Zhang, Removal of phosphate from aqueous solution by magnetic Fe–Zr binary oxide, Chem. Eng. J. 171 (2011) 448–455.
[12] W.W. Tang, G.M. Zeng, J.L. Gong, J. Liang, P. Xu, C. Zhang, B.B. Huang, Impact of humic/fulvic acid on the removal of heavy metals from aqueous solutions using nanomaterials: a review, Sci. Total Environ. 468–469 (2014) 1014–1027.
[13] X. Tan, Y. Liu, G. Zeng, X. Wang, X. Hu, Y. Gu, Z. Yang, Application of biochar for the removal of pollutants from aqueous solutions, Chemosphere 125 (2015) 70–85.
[14] R. Rajesh, E. Sujanthi, S. Senthil Kumar, R. Venkatesan, Designing versatile heterogeneous catalysts based on Ag and Au nanoparticles decorated on chitosan functionalized graphene oxide, Phys. Chem. Chem. Phys. 17 (2015) 11329–11340.
[15] P. Zhao, X. Feng, D. Huang, G. Yang, D. Astruc, Basic concepts and recent advances in nitrophenol reduction by gold- and other transition metal nanoparticles, Coord. Chem. Rev. 287 (2015) 114–136.
[16] Y. Fu, T. Huang, B. Jia, J. Zhu, X. Wang, Reduction of nitrophenols to aminophenols under concerted catalysis by Au/g-C_3N_4 contact system, Appl. Catal. B 202 (2017) 430–437.
[17] L. Qin, G. Zeng, C. Lai, D. Huang, C. Zhang, P. Xu, T. Hu, X. Liu, M. Cheng, Y. Liu, A visual application of gold nanoparticles: simple, reliable and sensitive detection of kanamycin based on hydrogen-bonding recognition, Sens. Actuat. B: Chem. 243 (2017) 946–954.
[18] Q. Ji, J.P. Hill, K. Ariga, Shell-adjustable hollow 'soft' silica spheres as a support for gold nanoparticles, J. Mater. Chem. A 1 (2013) 3600.
[19] J. Hu, Y.-L. Dong, X.-J. Chen, H.-J. Zhang, J.-M. Zheng, Q. Wang, X.-G. Chen, A highly efficient catalyst: in situ growth of Au nanoparticles on graphene oxide–Fe_3O_4 nanocomposite support, Chem. Eng. J. 236 (2014) 1–8.
[20] J. Zheng, Y. Dong, W. Wang, Y. Ma, J. Hu, X. Chen, X. Chen, In situ loading of gold nanoparticles on Fe_3O_4@SiO_2 magnetic nanocomposites and their high catalytic activity, Nanoscale 5 (2013) 4894–4901.
[21] B. Le Droumaguet, R. Poupart, D. Grande, "Clickable" thiol-functionalized nanoporous polymers: from their synthesis to further adsorption of gold nanoparticles and subsequent use as efficient catalytic supports, Polym. Chem. 6 (2015) 8105–8111.
[22] F. Cárdenas-Lizana, Z.M.D. Pedro, S. Gómez-Quero, L. Kiwi-Minsker, M.A. Keane, Carbon supported gold and silver: application in the gas phase hydrogenation of m-dinitrobenzene, J. Mol. Catal. A: Chem. 408 (2015) 138–146.
[23] F. Ke, J. Zhu, L.-G. Qiu, X. Jiang, Controlled synthesis of novel Au@MIL-100(Fe) core-shell nanoparticles with enhanced catalytic performance, Chem. Commun. 49 (2013) 1267–1269.
[24] A.D. Quast, M. Bornstein, B.J. Greydanus, I. Zharov, J.S. Shumaker-Parry, Robust polymer-coated diamond supports for noble-metal nanoparticle catalysts, ACS Catal. 6 (2016) 4729–4738.
[25] J.-H. Deng, X.-R. Zhang, G.-M. Zeng, J.-L. Gong, Q.-Y. Niu, J. Liang, Simultaneous removal of Cd(II) and ionic dyes from aqueous solution using magnetic graphene

oxide nanocomposite as an adsorbent, Chem. Eng. J. 226 (2013) 189–200.
[26] J.-L. Gong, B. Wang, G.-M. Zeng, C.-P. Yang, C.-G. Niu, Q.-Y. Niu, W.-J. Zhou, Y. Liang, Removal of cationic dyes from aqueous solution using magnetic multi-wall carbon nanotube nanocomposite as adsorbent, J. Hazard. Mater. 164 (2009) 1517–1522.
[27] H. Yi, D. Huang, G. Zeng, C. Lai, L. Qin, M. Cheng, S. Ye, B. Song, X. Ren, X. Guo, Selective prepared carbon nanomaterials for advanced photocatalytic application in environmental pollutant treatment and hydrogen production, Appl. Catal. B: Environ. (239) (2018) 408–424.
[28] X. Du, C. Li, L. Zhao, J. Zhang, L. Gao, J. Sheng, Y. Yi, J. Chen, G. Zeng, Promotional removal of HCHO from simulated flue gas over Mn-Fe oxides modified activated coke, Appl. Catal. B: Environ. 232 (2018) 37–48.
[29] S. Álvarez-Torrellas, M. Martin-Martinez, H.T. Gomes, G. Ovejero, J. García, Enhancement of p-nitrophenol adsorption capacity through N_2-thermal-based treatment of activated carbons, Appl. Surf. Sci. 414 (2017) 424–434.
[30] H. Chen, D. He, Q. He, P. Jiang, G. Zhou, W. Fu, Selective hydrogenation of p-chloronitrobenzene over an Fe promoted Pt/AC catalyst, RSC Adv. 7 (2017) 29143–29148.
[31] Y. Xie, C. Li, L. Zhao, J. Zhang, G. Zeng, X. Zhang, W. Zhang, S. Tao, Experimental study on Hg^0 removal from flue gas over columnar MnO_x-CeO_2/activated coke, Appl. Surf. Sci. 333 (2015) 59–67.
[32] S. Tao, C. Li, X. Fan, G. Zeng, P. Lu, X. Zhang, Q. Wen, W. Zhao, D. Luo, C. Fan, Activated coke impregnated with cerium chloride used for elemental mercury removal from simulated flue gas, Chem. Eng. J. 210 (2012) 547–556.
[33] B.F. Machado, P. Serp, Graphene-based materials for catalysis, Catal. Sci. Technol. 2 (2012) 54–75.
[34] P. Zhang, C. Shao, Z. Zhang, M. Zhang, J. Mu, Z. Guo, Y. Liu, TiO_2@carbon core/shell nanofibers: controllable preparation and enhanced visible photocatalytic properties, Nanoscale 3 (2011) 2943–2949.
[35] C. Lai, M.-M. Wang, G.-M. Zeng, Y.-G. Liu, D.-L. Huang, C. Zhang, R.-Z. Wang, P. Xu, M. Cheng, C. Huang, H.-P. Wu, L. Qin, Synthesis of surface molecular imprinted TiO_2/graphene photocatalyst and its highly efficient photocatalytic degradation of target pollutant under visible light irradiation, Appl. Surf. Sci. 390 (2016) 368–376.
[36] J. Sheng, C. Li, L. Zhao, X. Du, L. Gao, G. Zeng, Efficient removal of HCHO from simulated coal combustion flue gas using CuO-CeO_2 supported on cylindrical activated coke, Fuel 197 (2017) 397–406.
[37] K. Tong, Y. Zhang, D. Fu, X. Meng, Q. An, P.K. Chu, Removal of organic pollutants from super heavy oil wastewater by lignite activated coke, Colloids Surf. A: Physicochem. Eng. Asp. 447 (2014) 120–130.
[38] K. Tong, A. Lin, G. Ji, D. Wang, X. Wang, The effects of adsorbing organic pollutants from super heavy oil wastewater by lignite activated coke, J. Hazard Mater. 308 (2016) 113–119.
[39] H. Guo, Y. Ren, Q. Cheng, D. Wang, Y. Liu, Gold nanoparticles on cyanuric acid-based support: a highly active catalyst for the reduction of 4-nitrophenol in water, Catal. Commun. 102 (2017) 136–140.
[40] L. Ouarez, A. Chelouche, T. Touam, R. Mahiou, D. Djouadi, A. Potdevin, Au-doped ZnO sol-gel thin films: an experimental investigation on physical and photoluminescence properties, J. Lumin. 203 (2018) 222–229.
[41] F. Costanzo, M. Sulpizi, J. Vandevondele, R.G.D. Valle, M. Sprik, Ab initiomolecular dynamics study of ascorbic acid in aqueous solution, Mol. Phys. 105 (2007) 17–23.
[42] H. Li, Y. Liu, Y. Yang, D. Yang, J. Sun, Influences of hydrogen bonding dynamics on adsorption of ethyl mercaptan onto functionalized activated carbons: a DFT/TDDFT study, J. Photochem. Photobiol. A: Chrm. 291 (2014) 9–15.
[43] M. Nemanashi-Maumela, I. Nongwe, R.C. Motene, B.L. Davids, R. Meijboom, Au and Ag nanoparticles encapsulated within silica nanospheres using dendrimers as dual templating agent and their catalytic activity, Molecul. Catal. 438 (2017) 184–196.
[44] H. Sharififard, F. Zokaee Ashtiani, M. Soleimani, Adsorption of palladium and platinum from aqueous solutions by chitosan and activated carbon coated with chitosan, Asia-Pac. J. Chem. Eng. 8 (2013) 384–395.
[45] L. Qi, B. Cheng, J. Yu, W. Ho, High-surface area mesoporous Pt/TiO_2 hollow chains for efficient formaldehyde decomposition at ambient temperature, J. Hazard. Mater. 301 (2016) 522–530.
[46] Z. Li, L. Wu, H. Liu, H. Lan, J. Qu, Improvement of aqueous mercury adsorption on activated coke by thiol-functionalization, Chem. Eng. J. 228 (2013) 925–934.
[47] S. Nellaiappan, A.S. Kumar, S. Nisha, K. Chandrasekara Pillai, In-situ preparation of Au(111) oriented nanoparticles trapped carbon nanofiber-chitosan modified electrode for enhanced bifunctional electrocatalysis and sensing of formaldehyde and hydrogen peroxide in neutral pH solution, Electrochim. Acta 249 (2017) 227–240.
[48] B. Adhikari, A. Biswas, A. Banerjee, Graphene oxide-based hydrogels to make metal nanoparticle-containing reduced graphene oxide-based functional hybrid hydrogels, ACS Appl. Mater. Interfaces 4 (2012) 5472–5482.
[49] S. Wang, Q. Zhao, H. Wei, J.Q. Wang, M. Cho, H.S. Cho, O. Terasaki, Y. Wan, Aggregation-free gold nanoparticles in ordered mesoporous carbons: toward highly active and stable heterogeneous catalysts, J. Am. Chem. Soc. 135 (2013) 11849–11860.
[50] M.-B. Li, S.-K. Tian, Z. Wu, R. Jin, Cu^{2+} induced formation of $Au_{44}(SC_2H_4Ph)_{32}$ and its high catalytic activity for the reduction of 4-nitrophenol at low temperature, Chem. Commun. 51 (2015) 4433–4436.
[51] F. Zhang, X. Zhao, C. Feng, B. Li, T. Chen, W. Lu, X. Lei, S. Xu, Crystal-face-selective supporting of gold nanoparticles on layered double hydroxide as efficient catalyst for epoxidation of styrene, ACS Catal. 1 (2011) 232–237.
[52] X. Hu, B. Liu, Y. Deng, H. Chen, S. Luo, C. Sun, P. Yang, S. Yang, Adsorption and heterogeneous Fenton degradation of 17α-methyltestosterone on nano Fe_3O_4/MWCNTs in aqueous solution, Appl. Catal. B: Environ. 107 (2011) 274–283.
[53] D. Huang, C. Hu, G. Zeng, M. Cheng, P. Xu, X. Gong, R. Wang, W. Xue, Combination of Fenton processes and biotreatment for wastewater treatment and soil remediation, Sci. Total Environ. 574 (2017) 1599–1610.
[54] L. Li, M. Chen, G. Huang, N. Yang, L. Zhang, H. Wang, Y. Liu, W. Wang, J. Gao, A green method to prepare Pd–Ag nanoparticles supported on reduced graphene oxide and their electrochemical catalysis of methanol and ethanol oxidation, J. Power Sour. 263 (2014) 13–21.
[55] F. Montagne, J. Polesel-Maris, R. Pugin, H. Heinzelmann, Poly(N-isopropylacrylamide) thin films densely grafted onto gold surface: preparation, characterization, and dynamic AFM study of temperature-induced chain conformational changes, Langmuir 25 (2009) 983–991.
[56] F. Wei, J. Liu, Y.-N. Zhu, X.-S. Wang, C.-Y. Cao, W.-G. Song, In situ facile loading of noble metal nanoparticles on polydopamine nanospheres via galvanic replacement reaction for multifunctional catalysis, Sci. China Chem. 60 (2017) 1236–1242.
[57] F. Ali, S.B. Khan, T. Kamal, Y. Anwar, K.A. Alamry, A.M. Asiri, Bactericidal and catalytic performance of green nanocomposite based-on chitosan/carbon black fiber supported monometallic and bimetallic nanoparticles, Chemosphere 188 (2017) 588–598.
[58] S. Praharaj, S. Nath, S.K. Ghosh, S. Kundu, T. Pal, Immobilization and recovery of au nanoparticles from anion exchange resin: resin-bound nanoparticle matrix as a catalyst for the reduction of 4-nitrophenol, Langmuir 20 (2004) 9889–9892.
[59] Y. Deng, Y. Cai, Z. Sun, J. Liu, C. Liu, J. Wei, W. Li, C. Liu, Y. Wang, D. Zhao, Multifunctional mesoporous composite microspheres with well-designed nanostructure: a highly integrated catalyst system, J. Am. Chem. Soc. 132 (2010) 8466–8473.
[60] Y. Liu, L. Xu, X. Liu, M. Cao, Hybrids of gold nanoparticles with core-shell hyperbranched polymers: synthesis, characterization, and their high catalytic activity for reduction of 4-nitrophenol, Catalysts 6 (2015) 3.
[61] Y. Qiu, Z. Ma, P. Hu, Environmentally benign magnetic chitosan/Fe_3O_4 composites as reductant and stabilizer for anchoring Au NPs and their catalytic reduction of 4-nitrophenol, J. Mater. Chem. A 2 (2014) 13471–13478.
[62] W. Zhao, L. Xie, M. Zhang, Z. Ai, H. Xi, Y. Li, Q. Shi, J. Chen, Enhanced photocatalytic activity of all-solid-state g-C_3N_4/Au/P_{25} Z-scheme system for visible-light-driven H2 evolution, Int. J. Hydrog. Energy 41 (2016) 6277–6287.
[63] L. Rout, A. Kumar, R.S. Dhaka, G.N. Reddy, S. Giri, P. Dash, Bimetallic Au-Cu alloy nanoparticles on reduced graphene oxide support: synthesis, catalytic activity and investigation of synergistic effect by DFT analysis, Appl. Catal. A: Gen. 538 (2017) 107–122.
[64] Y. Choi, H.S. Bae, E. Seo, S. Jang, K.H. Park, B.-S. Kim, Hybrid gold nanoparticle-reduced graphene oxide nanosheets as active catalysts for highly efficient reduction of nitroarenes, J. Mater. Chem. 21 (2011) 15431.
[65] P. Guo, L. Tang, J. Tang, G. Zeng, B. Huang, H. Dong, Y. Zhang, Y. Zhou, Y. Deng, L. Ma, S. Tan, Catalytic reduction-adsorption for removal of p-nitrophenol and its conversion p-aminophenol from water by gold nanoparticles supported on oxidized mesoporous carbon, J. Colloid Interface Sci. 469 (2016) 78–85.
[66] P. Zhang, C. Shao, X. Li, M. Zhang, X. Zhang, C. Su, N. Lu, K. Wang, Y. Liu, An electron-rich free-standing carbon@Au core-shell nanofiber network as a highly active and recyclable catalyst for the reduction of 4-nitrophenol, Phys. Chem. Chem. Phys. 15 (2013) 10453–10458.
[67] X. Wang, J. Fu, M. Wang, Y. Wang, Z. Chen, J. Zhang, J. Chen, Q. Xu, Facile synthesis of Au nanoparticles supported on polyphosphazene functionalized carbon nanotubes for catalytic reduction of 4-nitrophenol, J. Mater. Sci. 49 (2014) 5056–5065.
[68] K. Layek, M.L. Kantam, M. Shirai, D. Nishio-Hamane, T. Sasaki, H. Maheswaran, Gold nanoparticles stabilized on nanocrystalline magnesium oxide as an active catalyst for reduction of nitroarenes in aqueous medium at room temperature, Green Chem. 14 (2012) 3164.
[69] X. Li, Y. Ma, Z. Yang, D. Huang, S. Xu, T. Wang, Y. Su, N. Hu, Y. Zhang, In situ preparation of magnetic Ni-Au/graphene nanocomposites with electron-enhanced catalytic performance, J. Alloy. Compd. 706 (2017) 377–386.
[70] V.K. Gupta, N. Atar, M.L. Yola, Z. Ustundag, L. Uzun, A novel magnetic Fe@Au core-shell nanoparticles anchored graphene oxide recyclable nanocatalyst for the reduction of nitrophenol compounds, Water Res. 48 (2014) 210–217.
[71] L. Qin, D. Huang, P. Xu, G. Zeng, C. Lai, Y. Fu, H. Yi, B. Li, C. Zhang, M. Cheng, C. Zhou, X. Wen, In-situ deposition of gold nanoparticles onto polydopamine-decorated g-C_3N_4 for highly efficient reduction of nitroaromatics in environmental water purification, J. Colloid Interface Sci. 534 (2018) 357–369.
[72] X. Zhou, C. Lai, D. Huang, G. Zeng, L. Chen, L. Qin, P. Xu, M. Cheng, C. Huang, C. Zhang, Preparation of water-compatible molecularly imprinted thiol-functionalized activated titanium dioxide: selective adsorption and efficient photodegradation of 2,4-dinitrophenol in aqueous solution, J. Hazard. Mater. 346 (2018) 113–123.
[73] J. Xia, G. He, L. Zhang, X. Sun, X. Wang, Hydrogenation of nitrophenols catalyzed by carbon black-supported nickel nanoparticles under mild conditions, Appl. Catal. B: Environ. 180 (2016) 408–415.
[74] S. Wunder, F. Polzer, Y. Lu, Y. Mei, M. Ballauff, Kinetic analysis of catalytic reduction of 4-nitrophenol by metallic nanoparticles immobilized in spherical polyelectrolyte brushes, J. Phys. Chem. C 114 (2010) 8814–8820.
[75] T. Aditya, A. Pal, T. Pal, Nitroarene reduction: a trusted model reaction to test nanoparticle catalysts, Chem. Commun. (Camb.) 51 (2015) 9410–9431.
[76] W. Xie, B. Walkenfort, S. Schlücker, Label-free SERS monitoring of chemical reactions catalyzed by small gold nanoparticles using 3D plasmonic superstructures, J. Am. Chem. Soc. 135 (2013) 1657–1660.
[77] Q. Cui, B. Xia, S. Mitzscherling, A. Masic, L. Li, M. Bargheer, H. Möhwald, Preparation of gold nanostars and their study in selective catalytic reactions, Colloids Surf. A: Physicochem. Eng. Asp. 465 (2015) 20–25.
[78] S. Biella, L. Prati, M. Rossi, Selective oxidation of D-glucose on gold catalyst, J.

Catal. 206 (2002) 242–247.
[79] H. Zhang, D. Chen, X. Lv, Y. Wang, H. Chang, J. Li, Energy-efficient photodegradation of azo dyes with TiO_2 nanoparticles based on photoisomerization and alternate UV – visible light, Environ. Sci. Technol. 44 (2010) 1107–1111.
[80] M. Chen, P. Xu, G. Zeng, C. Yang, D. Huang, J. Zhang, Bioremediation of soils contaminated with polycyclic aromatic hydrocarbons, petroleum, pesticides, chlorophenols and heavy metals by composting: applications, microbes and future research needs, Biotechnol. Adv. 33 (2015) 745–755.
[81] C. Umamaheswari, A. Lakshmanan, N.S. Nagarajan, Green synthesis, characterization and catalytic degradation studies of gold nanoparticles against congo red and methyl orange, J. Photochem. Photobiol. B 178 (2018) 33–39.
[82] U. Tyagi, N. Anand, D. Kumar, Synergistic effect of modified activated carbon and ionic liquid in the conversion of microcrystalline cellulose to 5-Hydroxymethyl Furfural, Bioresour. Technol. 267 (2018) 326–332.
[83] Y. Zhu, X. Cao, Y. Cheng, T. Zhu, Performances and structures of functional microbial communities in the mono azo dye decolorization and mineralization stages, Chemosphere 210 (2018) 1051–1060.
[84] W. Zhong, T. Jiang, Y. Dang, J. He, S.-Y. Chen, C.-H. Kuo, D. Kriz, Y. Meng, A.G. Meguerdichian, S.L. Suib, Mechanism studies on methyl orange dye degradation by perovskite-type $LaNiO_3$-δ under dark ambient conditions, Appl. Catal. A: Gen. 549 (2018) 302–309.
[85] N. Srivastava, M. Mukhopadhyay, Biosynthesis of SnO_2 nanoparticles using bacterium erwinia herbicola and their photocatalytic activity for degradation of dyes, Ind. Eng. Chem. Res. 53 (2014) 13971–13979.
[86] J. Hu, Y.-L. Dong, Z.U. Rahman, Y.-H. Ma, C.-L. Ren, X.-G. Chen, In situ preparation of core-satellites nanostructural magnetic-Au NPs composite for catalytic degradation of organic contaminants, Chem. Eng. J. 254 (2014) 514–523.